Synthesis, Characterization, and Magnetic Studies of Two Novel Isostructural Pentanuclear Iron(II) Complexes

Susanna Herold and Stephen J. Lippard*

Department of Chemistry, Massachusetts Institute of Technology, Cambridge, Massachusetts 02139

Received July 3, 1996[⊗]

The synthesis, X-ray structural characterization, and Mössbauer and magnetic properties of the two pentanuclear complexes $[Fe_5(\mu_3\text{-}F)_2(XDK)_2(L)_4(O_2CPh)_4]$, where L = pyridine (py) or *N*-methylimidazole (*N*-MeIm), are described. Reaction of $[Fe(H_2O)_6](BF_4)_2$, the deprotonated dinucleating dicarboxylate ligand XDK, H_2XDK = *m*-xylylenediamine bis(Kemp's triacid)imide, benzoate, and a nitrogen donor ligand, py or *N*-MeIm, afforded $[Fe_5(\mu_3\text{-}F)_2(XDK)_2(py)_4(O_2CPh)_4]$ (**1**) and $[Fe_5(\mu_3\text{-}F)_2(XDK)_2(N\text{-}MeIm)_4(O_2CPh)_4]$ (**2**), respectively. Complex **1**·$4CH_2Cl_2$ crystallizes in the triclinic space group $P\bar{1}$, with $a = 13.1474(8)$ Å, $b = 15.081(1)$ Å, $c = 16.560(1)$ Å, $\alpha = 98.807(6)°$, $\beta = 111.242(6)°$, $\gamma = 93.723(5)°$, $V = 2998.4(4)$ Å^3, and $Z = 1$ ($R = 0.084$, $R_w = 0.084$), and complex **2**·$2Et_2O$ crystallizes in the monoclinic space group $P2_1/n$, with $a = 20.641(3)$ Å, $b = 13.845(2)$ Å, $c = 21.170(4)$ Å, $\beta = 102.56(1)°$, $V = 5905(2)$ Å^3, and $Z = 2$ ($R = 0.066$, $R_w = 0.082$). In both complexes, the five iron atoms occupy the corners of two equivalent, nearly equilateral triangles with one vertex in common, which is situated on a crystallographic inversion center. A triply-bridging fluoride ion is located in the center of each triangle, raised slightly (∼0.18 Å) above the plane formed by the three iron atoms. The coordination spheres of the four outer iron ions are trigonal bipyramidal, whereas the central iron displays an octahedral coordination geometry. The inequivalence of the iron atoms is reflected by the presence of two overlapping quadrupole doublets, with an approximate intensity ratio of 4:1, in the Mössbauer spectra of the two complexes ($\delta_1 = 1.25$ mm/s, $\delta_2 = 1.30$ mm/s, $\Delta E_{Q1} = 2.80$ mm/s, and $\Delta E_{Q2} = 2.06$ mm/s for **1** and $\delta_1 = 1.32$ mm/s, $\delta_2 = 1.42$ mm/s, $\Delta E_{Q1} = 3.14$ mm/s, and $\Delta E_{Q2} = 2.85$ mm/s for **2**). Conductivity and Mössbauer measurements of methanol solutions of **1** suggested partial dissociation of the complex, probably of the benzoate ligands. Magnetic susceptibility data for both compounds **1** and **2** at 5000 G in the temperature range 4−300 K revealed a decrease in the effective moment with decreasing temperature. The molar magnetic susceptibility versus temperature plots could be fit with a simplified theoretical model obtained by considering two different exchange pathways, consistent with the symmetry of the molecule.

Introduction

The growing interest in metalloproteins with non-heme carboxylate-bridged diiron sites[1] has stimulated, over the past few years, many studies of the chemistry of iron carboxylate complexes. Significant examples of proteins in this class that have been crystallographically characterized in both the reduced and oxidized forms are hemerythrin,[2,3] the R2 protein of ribonucleotide reductase,[4−6] and the hydroxylase component of methane monooxygenase.[7,8] A large number of carboxylate-bridged diiron(III) complexes have been prepared as models for the active sites of these proteins.[9−14] Lately, the focus of interest has moved toward the synthesis of diiron(II) complexes, in particular, to prepare functional models for methane monooxygenase.[15−26] The reduced form of this enzyme is responsible for the dioxygen activation chemistry.

One strategy for preparing carboxylate-bridged diiron(II) complexes has been to use the dinucleating dicarboxylate ligand *m*-xylylenediamine bis(Kemp's triacid)imide (H_2XDK). This ligand has facilitated the synthesis of $\{Fe_2(XDK)\}$ complexes with a variety of different third bridging ligands including chloride, fluoride, triflate, and benzoate.[25] By using the ligand XDK, we have also prepared two novel isostructural carboxyl-

[⊗] Abstract published in *Advance ACS Abstracts,* December 15, 1996.

(1) Nordlund, P.; Eklund, H. *Curr. Opin. Struct. Biol.* **1995**, *5*, 758−766.
(2) Holmes, M. A.; Le Trong, I.; Turley, S.; Sieker, L. C.; Stenkamp, R. E. *J. Mol. Biol.* **1991**, *218*, 583−593.
(3) Holmes, M. A.; Stenkamp, R. E. *J. Mol. Biol.* **1991**, *220*, 723−737.
(4) Nordlund, P.; Sjöberg, B.-M.; Eklund, H. *Nature* **1990**, *345*, 593−598.
(5) Nordlund, P.; Eklund, H. *J. Mol. Biol.* **1993**, *232*, 123−164.
(6) Åberg, A. Thesis, Stockholm University, 1993.
(7) Rosenzweig, A. C.; Frederick, C. A.; Lippard, S. J.; Nordlund, P. *Nature* **1993**, *366*, 537−543.
(8) Rosenzweig, A. C.; Nordlund, P.; Takahara, P. M.; Frederick, C. A.; Lippard, S. J. *Chem. Biol.* **1995**, *2*, 409−418.
(9) Lippard, S. J. *Angew. Chem., Int. Ed. Engl.* **1988**, *27*, 344−361.
(10) Sanders-Loehr, J. In *Iron Carriers and Iron Proteins*; Loehr, T. M., Ed.; VCH Press: New York, 1989; pp 373−466.
(11) Vincent, J. B.; Olivier-Lilley, G. L.; Averill, B. A. *Chem. Rev.* **1990**, *90*, 1447−1467.
(12) Kurtz, D. M., Jr. *Chem. Rev.* **1990**, *90*, 585−606.
(13) Que, L., Jr.; True, A. E. *Prog. Inorg. Chem.* **1990**, *38*, 97−200.
(14) Que, L., Jr. In *Bioinorganic Catalysis*; Reedijk, J., Ed.; Dekker: New York, 1993; pp 347−393.
(15) Feig, A. L.; Lippard, S. J. *Chem. Rev.* **1994**, *94*, 759−805.
(16) Que, L., Jr.; Dong, Y. *Acc. Chem. Res.* **1996**, *29*, 190−196.
(17) Hartman, J. R.; Rardin, R. L.; Chaudhuri, P.; Pohl, K.; Wieghardt, K.; Nuber, B.; Weiss, J.; Papaefthymiou, G. C.; Frankel, R. B.; Lippard, S. J. *J. Am. Chem. Soc.* **1987**, *109*, 7387−7396.
(18) Tolman, W. B.; Liu, S.; Bentsen, J. G.; Lippard, S. J. *J. Am. Chem. Soc.* **1991**, *113*, 152−164.
(19) Stassinopoulos, A.; Schulte, G.; Papaefthymiou, G. C.; Caradonna, J. P. *J. Am. Chem. Soc.* **1991**, *113*, 8686−8697.
(20) Kitajima, N.; Tamura, N.; Tanaka, M.; Moro-oka, Y. *Inorg. Chem.* **1992**, *31*, 3342−3343.
(21) Ménage, S.; Zang, Y.; Hendrich, M. P.; Que, L., Jr. *J. Am. Chem. Soc.* **1992**, *114*, 7786−7792.
(22) Hayashi, Y.; Suzuki, M.; Uehara, A.; Mizutani, Y.; Kitagawa, T. *Chem. Lett.* **1992**, 91−94.
(23) Hagen, K. S.; Lachicotte, R. *J. Am. Chem. Soc.* **1992**, *114*, 8741−8742.
(24) Dong, Y.; Ménage, S.; Brennan, B. A.; Elgren, T. E.; Jang, H. G.; Pearce, L. L.; Que, L., Jr. *J. Am. Chem. Soc.* **1993**, *115*, 1851−1859.
(25) Herold, S.; Pence, L. E.; Lippard, S. J. *J. Am. Chem. Soc.* **1995**, *117*, 6134−6135.
(26) Coucouvanis, D.; Reynolds, R. A., III; Dunham, W. R. *J. Am. Chem. Soc.* **1995**, *117*, 7570−7571.

S0020-1669(96)00783-5 CCC: $14.00

ate-bridged pentanuclear iron(II) complexes, the synthesis and properties of which form the basis for the present article.

Attempts to understand both the structure and the mechanism of non-heme iron proteins through the study of model compounds have led to the discovery of a variety of polynuclear iron(III) complexes, with nuclearity up to Fe_{19}.[27−30] The polyiron cores of these complexes exhibit an array of geometries and have been investigated as possible intermediates in the formation of the core of the iron storage protein ferritin (Ft). Mixed-valent iron(II)/iron(III) forms are also thought to form during growth of the Ft core, and a few mixed-valent high-nuclearity iron complexes, up to Fe_{12}, have been described as models for this process.[31−34] The number of polynuclear iron(II) compounds is very small, however, and the nuclearity of the known complexes is not very high.[34−36] The largest aggregate reported to date is the octanuclear *N*,*N*-dialkylcarbamate complex $[\{Fe_4(\mu_4\text{-}O)(O_2CN^iPr_2)_6\}_2]$.[37]

Understanding the nature of magnetic exchange interactions in polynuclear complexes is a further point of interest. The increased complexity involved in performing theoretical analyses of large spin systems renders such studies particularly challenging. Interpreting the magnetic behavior of polynuclear iron(II) aggregates is further complicated by factors such as large anisotropy, zero-field splitting, and orbital contributions to the magnetization, properties typical of iron(II) ions.[38]

In this paper we describe the synthesis and the characterization of the two isostructural pentanuclear compounds $[Fe_5(\mu_3\text{-}F)_2(XDK)_2(L)_4(O_2CPh)_4]$, where L = pyridine (**1**) or *N*-methylimidazole (**2**). In this new type of polyiron(II) aggregate, the five iron(II) ions are arranged in two equivalent, nearly equilateral triangles which share a vertex. A triply-bridging fluoride ion, never encountered before in polyiron(II) complexes, is situated in the center of each triangle. Because of the high symmetry of the molecule, a simplified theoretical study of the magnetic properties of compounds **1** and **2** could be carried out, providing satisfactory fits for the magnetic susceptibility data. Conductivity and Mössbauer studies of polycrystalline and frozen solution samples indicated that only partial dissociation occurs in methanol.

Experimental Section

General Procedures and Methods. Solvents were dried and distilled under nitrogen by standard procedures. Unless otherwise noted, reagents were obtained from commercial suppliers and used as received. The ligand H_2XDK was prepared according to a literature procedure.[39−41] All manipulations and reactions were carried out under an inert atmosphere in a Vacuum Atmospheres glovebox. IR spectra in the range 4000−400 cm^{-1} were obtained and manipulated by using a Bio-Rad SPC3200 FTIR instrument. Conductivity measurements were carried out in methanol with a Fisher Scientific conductivity bridge Model 9-326 with a platinum-black electrode. Molar conductivities were derived from the slopes of conductivity (μS/cm) versus concentration plots. The assignment of electrolyte type was determined by reference to the molar conductivities of $[n\text{-}Bu_4N]PF_6$ and $[Fe(H_2O)_6](BF_4)_2$ in methanol.

Table 1. X-ray Crystallographic Information for $[Fe_5(\mu_3\text{-}F)_2(XDK)_2(py)_4(O_2CPh)_4]\cdot 4CH_2Cl_2$ (**1**·$4CH_2Cl_2$) and $[Fe_5(\mu_3\text{-}F)_2(XDK)_2(N\text{-}MeIm)_4(O_2CPh)_4]\cdot 2Et_2O$ (**2**·$2Et_2O$)

	1·$4CH_2Cl_2$	**2**·$2Et_2O$
formula	$Fe_5C_{116}H_{124}N_8O_{24}Cl_8F_2$	$Fe_5C_{116}H_{140}N_{12}O_{26}F_2$
mol wt (g mol^{-1})	2615.15	2435.68
cryst system	triclinic	monoclinic
space group	$P\bar{1}$ (No. 2)	$P2_1/n$ (No. 14)
a (Å)	13.1474(8)	20.641(3)
b (Å)	15.081(1)	13.845(2)
c (Å)	16.560(1)	21.170(4)
α (deg)	98.807(6)	
β (deg)	111.242(6)	102.56(1)
γ (deg)	93.723(5)	
V (Å^3)	2998.4(4)	5905(2)
Z	1	2
radiation	Mo Kα, λ = 0.716 09 Å	Mo Kα, λ = 0.710 69 Å
ρ_{calc} (g cm^{-3})	1.45	1.37
temperature (K)	198	163
μ (cm^{-1})	8.44	6.79
transmission coeff	0.999−0.916	0.999−0.840
2θ range, deg	$3 < 2\theta < 54$	$3 < 2\theta < 50$
index range	$+h, \pm k, \pm l$	$+h, +k, \pm l$
total no. of data	12 978	11 472
no. of unique data[a]	4739	4544
no. of parameters	641	572
R[b]	0.084	0.066
R_w[c]	0.084	0.082
largest shift/esd, final	0.000	0.000
largest peak, e$^-$/Å^3	0.9	0.58

[a] Observation criterion $I > 3\sigma(I)$. [b] $R = \sum||F_o| - |F_c||/\sum|F_o|$. [c] $R_w = [\sum w(|F_o| - |F_c|)^2/\sum w|F_o|^2]^{1/2}$, where $w = 1/\sigma^2(F_o)$.

Synthetic Procedures. $[Fe_5(\mu_3\text{-}F)_2(XDK)_2(py)_4(O_2CPh)_4]$ (1). A solution of H_2XDK (116 mg, 0.2 mmol) and Et_3N (40 mg, 0.4 mmol) in CH_2Cl_2 (5 mL) was added to a solution of $[Fe(H_2O)_6](BF_4)_2$ (169 mg, 0.5 mmol) in MeOH (5 mL). Subsequent addition of distilled pyridine (32 mg, 0.4 mmol) in CH_2Cl_2 (5 mL) and a solution of $(Me_4N)(O_2CPh)$ (98 mg, 0.5 mmol) in MeOH (5 mL) yielded a deep yellow reaction mixture. After the mixture was stirred for 2 h, the precipitated BF_4^- salts were filtered, and the solution was evaporated to dryness. The deep yellow residue was dissolved in CH_2Cl_2 (2 mL), filtered again, and layered with Et_2O (∼15 mL). After a few days, $[Fe_5(\mu_3\text{-}F)_2(XDK)_2(py)_4(O_2CPh)_4]$ (**1**), deposited as a deep yellow crystalline material, was collected, washed with Et_2O, and dried (174 mg, 75%). Crystals of **1**·$4CH_2Cl_2$ suitable for X-ray diffraction analysis were grown by slow diffusion of Et_2O into a CH_2Cl_2 solution of **1**. FTIR (KBr, cm^{-1}): 3506, 3130, 3062, 2968, 2930, 2775, 2741, 1734, 1695, 1605, 1570, 1465, 1444, 1405, 1395, 1360, 1229, 1218, 1190, 1087, 1069, 1040, 958, 872, 851, 828, 736, 719, 699, 658, 620, 480, 471, 450, 425. Anal. Calcd for **1**·$0.5CH_2Cl_2$, $C_{112}H_{116}N_8O_{24}F_2Fe_5\cdot 0.5CH_2Cl_2$ (2317.89): C, 58.30; H, 5.09; N, 4.83; F, 1.64. Found: C, 58.25; H, 5.14; N, 4.89; F, 1.91.

$[Fe_5(\mu_3\text{-}F)_2(XDK)_2(N\text{-}MeIm)_4(O_2CPh)_4]$ (2). The procedure described above for the preparation of **1** was applied also for the synthesis of **2**, except that distilled *N*-methylimidazole (32 mg, 0.4 mmol) was added as the nitrogen donor ligand. After the reaction mixture was stirred for 2 h, the precipitated BF_4^- salts were filtered, and the solution was evaporated to dryness. The deep yellow residue was dissolved in

(27) Hagen, K. S. *Angew. Chem., Int. Ed. Engl.* **1992**, *31*, 1010−1012.
(28) Heath, S. L.; Powell, A. K. *Angew. Chem., Int. Ed. Engl.* **1992**, *31*, 191−193.
(29) (a) Gorun, S. M.; Papaefthymiou, G. C.; Frankel, R. B.; Lippard, S. J. *J. Am. Chem. Soc.* **1987**, *109*, 3337−3348. (b) Micklitz, W.; McKee, V.; Rardin, R. L.; Pence, L. E.; Papaefthymiou, G. C.; Bott, S. G.; Lippard, S. J. *J. Am. Chem. Soc.* **1994**, *116*, 8061−8069.
(30) Powell, A. K.; Heath, S. L.; Gatteschi, D.; Pardi, L.; Sessoli, R.; Spina, G.; Del Giallo, F.; Pieralli, F. *J. Am. Chem. Soc.* **1995**, *117*, 2491−2502.
(31) Caneschi, A.; Cornia, A.; Lippard, S. J.; Papaefthymiou, G. C.; Sessoli, R. *Inorg. Chim. Acta* **1996**, *243*, 295−304.
(32) Taft, K. L.; Papaefthymiou, G. C.; Lippard, S. J. *Science* **1993**, *259*, 1302−1305.
(33) Taft, K. L.; Papaefthymiou, G. C.; Lippard, S. J. *Inorg. Chem.* **1994**, *33*, 1510−1520.
(34) Taft, K. L.; Caneschi, A.; Pence, L. E.; Delfs, C. D.; Papaefthymiou, G. C.; Lippard, S. J. *J. Am. Chem. Soc.* **1993**, *115*, 11753−11766.
(35) Shoner, S. C.; Power, P. P. *Inorg. Chem.* **1992**, *31*, 1001−1010.
(36) Ménage, S.; Fujii, H.; Hendrich, M. P.; Que, L., Jr. *Angew. Chem., Int. Ed. Engl.* **1994**, *33*, 1660−1662.
(37) Belli Dell'Amico, D.; Calderazzo, F.; Labella, L.; Maichle-Mössmer, C.; Strähle, J. *J. Chem. Soc., Chem. Commun.* **1994**, 1555−1556.
(38) Carlin, R. L. *Magnetochemistry*; Springer-Verlag: New York, 1986.
(39) Watton, S. P.; Masschelein, A.; Rebek, J., Jr.; Lippard, S. J. *J. Am. Chem. Soc.* **1994**, *116*, 5196−5205.
(40) Rebek, J., Jr.; Marshall, L.; Wolak, R.; Parris, K.; Killoran, M.; Askew, B.; Nemeth, D.; Islam, N. *J. Am. Chem. Soc.* **1985**, *107*, 7476−7481.
(41) Marshall, L.; Parris, K.; Rebek, J., Jr.; Luis, S. V.; Burguete, M. I. *J. Am. Chem. Soc.* **1988**, *110*, 5192−5193.

Table 2. Atomic Positional Parameters and Equivalent Isotropic Thermal Parameters for $[Fe_5(\mu_3\text{-}F)_2(XDK)_2(py)_4(O_2CPh)_4]\cdot 4CH_2Cl_2$ (**1**·$4CH_2Cl_2$)[a]

atom	*x*	*y*	*z*	B_{eq}[b]	atom	*x*	*y*	*z*	B_{eq}[b]
Fe(1)	0.1475(1)	0.1340(1)	0.7068(1)	1.97(4)	C(21)	−0.1464(9)	0.1432(8)	0.2772(8)	2.2(2)
Fe(2)	0.1535(1)	0.2091(1)	0.5135(1)	1.89(4)	C(22)	−0.258(1)	0.1222(10)	0.2571(10)	4.7(3)
Fe(3)	0	0	0	1.79(6)	C(23)	−0.331(1)	0.137(1)	0.173(1)	5.9(4)
F(1)	0.0867(5)	0.1187(4)	0.5703(4)	2.1(1)	C(24)	−0.291(1)	0.1729(9)	0.1199(9)	3.8(3)
O(10)	0.0129(6)	0.0659(5)	0.7094(5)	2.9(2)	C(25)	−0.183(1)	0.1903(9)	0.1405(9)	4.4(3)
O(11)	−0.1057(6)	0.0074(5)	0.5721(5)	2.7(2)	C(26)	−0.109(1)	0.1777(8)	0.2224(8)	3.0(3)
O(20)	−0.0992(6)	0.0702(5)	0.4018(5)	2.3(2)	C(101)	0.3349(9)	0.1295(8)	0.6410(8)	1.9(3)
O(21)	0.0224(6)	0.1803(5)	0.3986(5)	2.5(2)	C(102)	0.5550(9)	0.2705(9)	0.7001(8)	2.5(3)
O(101)	0.2965(6)	0.1262(5)	0.6992(5)	2.4(2)	C(103)	0.5388(9)	0.2064(8)	0.8294(8)	2.2(3)
O(102)	0.3021(6)	0.1713(5)	0.5792(5)	2.6(2)	C(104)	0.3681(10)	−0.0165(9)	0.5787(8)	3.5(3)
O(103)	0.5209(7)	0.2211(5)	0.8949(5)	3.1(2)	C(105)	0.643(1)	0.0835(9)	0.8827(8)	4.2(4)
O(104)	0.5409(8)	0.3345(6)	0.6637(6)	3.9(3)	C(106)	0.680(1)	0.2141(9)	0.6324(9)	4.5(4)
O(201)	0.1125(6)	0.2649(5)	0.7160(5)	2.3(2)	C(107)	0.4299(9)	0.0719(8)	0.6419(7)	2.2(3)
O(202)	0.1312(6)	0.3105(5)	0.6001(5)	2.1(2)	C(108)	0.4907(10)	0.0518(8)	0.7323(8)	2.9(3)
O(203)	0.2146(6)	0.4142(5)	0.9000(5)	2.7(2)	C(109)	0.585(1)	0.1237(8)	0.7993(8)	3.1(3)
O(204)	0.2700(7)	0.5183(5)	0.6752(6)	2.8(2)	C(110)	0.6623(9)	0.1485(8)	0.7563(8)	3.3(3)
N(1)	0.2251(8)	0.1375(7)	0.8460(7)	2.7(3)	C(111)	0.5997(10)	0.1878(9)	0.6725(8)	3.0(3)
N(2)	0.2293(8)	0.3098(7)	0.4645(7)	2.8(3)	C(112)	0.5103(10)	0.1150(8)	0.6079(8)	2.8(3)
N(101)	0.5235(7)	0.2721(6)	0.7745(6)	2.2(2)	C(201)	0.0886(9)	0.3095(7)	0.6557(8)	2.3(3)
N(201)	0.2392(7)	0.4650(6)	0.7846(6)	2.1(2)	C(202)	0.207(1)	0.5066(8)	0.7107(9)	2.8(3)
C(0)	0.291(1)	0.206(1)	0.9009(10)	5.2(4)	C(203)	0.178(1)	0.4464(8)	0.8353(8)	2.4(3)
C(1)	0.345(1)	0.208(1)	0.9908(10)	5.1(4)	C(204)	−0.1069(10)	0.3060(9)	0.5789(8)	3.2(3)
C(2)	0.333(1)	0.136(1)	1.0224(9)	4.9(4)	C(205)	0.093(1)	0.6142(9)	0.6365(9)	4.7(4)
C(3)	0.265(2)	0.062(1)	0.9676(9)	6.0(5)	C(206)	0.027(1)	0.495(1)	0.882(1)	5.1(5)
C(4)	0.208(1)	0.0667(10)	0.8796(9)	4.4(4)	C(207)	0.0053(10)	0.3695(8)	0.6487(8)	2.6(3)
C(5)	0.202(1)	0.3159(10)	0.3810(10)	3.8(4)	C(208)	0.0123(10)	0.4539(8)	0.6127(8)	3.3(3)
C(6)	0.246(1)	0.383(1)	0.351(1)	5.3(5)	C(209)	0.092(1)	0.5347(8)	0.6796(8)	2.9(3)
C(7)	0.322(2)	0.450(1)	0.411(1)	6.5(6)	C(210)	0.060(1)	0.5544(9)	0.7574(9)	3.6(3)
C(8)	0.352(1)	0.446(1)	0.500(1)	6.2(5)	C(211)	0.0613(10)	0.4757(10)	0.8034(9)	3.7(4)
C(9)	0.304(1)	0.373(1)	0.523(1)	4.9(4)	C(212)	−0.0208(10)	0.3950(9)	0.7359(9)	3.7(4)
C(10)	−0.0745(10)	0.0203(8)	0.6553(7)	2.1(3)	C(301)	0.3823(9)	0.3694(7)	0.7828(7)	1.8(2)
C(11)	−0.1472(9)	−0.0267(7)	0.6933(8)	2.1(2)	C(302)	0.4915(9)	0.3578(8)	0.8086(8)	2.4(2)
C(12)	−0.110(1)	−0.0204(9)	0.7827(9)	3.6(3)	C(303)	0.5737(10)	0.4235(8)	0.8664(8)	2.5(2)
C(13)	−0.169(1)	−0.071(1)	0.8211(10)	5.0(4)	C(304)	0.5413(10)	0.5019(8)	0.9035(8)	2.8(3)
C(14)	−0.270(1)	−0.120(1)	0.766(1)	4.9(4)	C(305)	0.432(1)	0.5156(8)	0.8791(8)	2.9(3)
C(15)	−0.307(1)	−0.1273(9)	0.6764(10)	4.1(3)	C(306)	0.3532(9)	0.4475(8)	0.8169(8)	2.2(2)
C(16)	−0.244(1)	−0.0785(9)	0.6390(8)	3.3(3)	C(307)	0.695(1)	0.4142(9)	0.8967(9)	4.3(4)
C(20)	−0.0688(9)	0.1292(8)	0.3685(7)	1.8(2)	C(308)	0.402(1)	0.6041(8)	0.9128(8)	3.3(3)

[a] Numbers in parentheses are errors in the last significant digit. See Figures S1 and S2 for atom-labeling scheme. [b] $B_{eq} = (4/3)[a^2\beta_{11} + b^2\beta_{22} + c^2\beta_{33} + 2ab\cos(\gamma)\beta_{12} + 2ac\cos(\beta)\beta_{13} + 2bc\cos(\alpha)\beta_{23}]$.

CH_2Cl_2 (2 mL), filtered, diluted with MeOH (1 mL), and layered with Et_2O (∼15 mL). After a few days, $[Fe_5(\mu_3\text{-}F)_2(XDK)_2(N\text{-}MeIm)_4(O_2CPh)_4]$ (**2**) deposited as a deep yellow crystalline material, was collected, washed with Et_2O, and dried (168 mg, 71%). The yellow crystals of **2** were sometimes contaminated with a colorless crystalline material identified as residual BF_4^- salts and/or the mononuclear complex $[Fe(HXDK)_2(MeOH)_2]$.[42] For the final purification, the mixture was dissolved in benzene, insoluble impurities were filtered off and the complex **2** was crystallized by layering with Et_2O. Crystals of **2**·$2Et_2O$ suitable for X-ray diffraction analysis were grown by slow diffusion of Et_2O into a MeOH solution of **2**. FTIR (KBr, cm^{-1}): 3437, 3135, 3061, 2962, 2929, 2776, 2740, 1733, 1691, 1609, 1571, 1534, 1460, 1400, 1361, 1336, 1285, 1244, 1229, 1195, 1109, 1087, 958, 887, 852, 828, 763, 720, 674, 659, 636, 618, 473, 448, 426. Anal. Calcd for **2**·Et_2O, $C_{108}H_{120}N_{12}O_{24}F_2Fe_5\cdot Et_2O$ (2361.56): C, 56.96; H, 5.55; N, 7.12; F, 1.61. Found: C, 56.58; H, 5.39; N, 6.79; F, 1.72.

X-ray Crystallography. General Procedures. X-ray diffraction studies were performed with an Enraf-Nonius CAD-4F Kappa geometry diffractometer and graphite-monochromatized Mo Kα radiation (λ = 0.710 69 Å) by using general procedures previously described.[43] The crystal temperature was maintained by the use of an Enraf-Nonius FR558-S liquid nitrogen cryostat. No appreciable decay was observed for the two compounds, as judged by periodic monitoring of the intensities of three standard reflections. A systematic search for higher symmetry was conducted by using TRACER and none was found.[44] Initial iron atomic coordinates were obtained by using the direct method program SHELXS-86.[45] The remaining heavy atoms were located with DIRDIF phase refinements and difference Fourier maps.[46] All calculations were performed with a VAXstation 4000-90 computer and the TEXSAN software package.[47] Hydrogen atoms were placed at calculated positions (C−H = 0.95 Å), with hydrogen thermal parameters set equal to $1.2B_{eq}$ of the atom to which they were bound. They were included but not refined in the final least-square cycles. Absorption corrections based on ψ scans were applied for both **1** and **2**.[48]

Crystallographic data are summarized in Table 1. Atomic coordinates and B_{eq} values for **1** and **2**, excluding those of lattice solvents and hydrogen atoms, are given in Tables 2 and 3, respectively. Selected bond distances and angles are given in Tables 4 and 5. Complete listings of atomic coordinates and B_{eq}, anisotropic thermal parameters, and intramolecular bond distances and angles are available as Supporting Information (Tables S1−S8), together with an ORTEP diagram of **2** and the numbering scheme for the XDK ligand (Figures S1 and S2, Supporting Information).

(42) The mononuclear complex $[Fe(HXDK)_2(MeOH)_2]$, often formed as a side product in reactions of iron(II) and the XDK ligand, was characterized by X-ray crystallography, Herold, S.; Lippard, S. J. *J. Am. Chem. Soc.*, in press.

(43) Carnahan, E. M.; Rardin, R. L.; Bott, S. G.; Lippard, S. J. *Inorg. Chem.* **1992**, *31*, 5193−5201.

(44) Lawton, S. L. *TRACER II: A Fortran Lattice Transformation-Cell Reduction Program*; Mobil Oil Corp.: Paulsboro, NJ, 1967.

(45) Sheldrick, G. M. *SHELX86. Program for crystal structure determination*; University of Göttingen: Göttingen, Germany, 1986.

(46) Parthasarathi, V.; Beurskens, P. T.; Slot, H. J. B. *Acta Crystallogr.* **1983**, *A39*, 860−864.

(47) TEXSAN: *Single Crystal Structure Analysis Software, Version 1.6*; Molecular Structure Corp.: The Woodlands, TX, 1993.

(48) North, A. C. T.; Phillips, D. C.; Mathews, F. S. *Acta Crystallogr.* **1968**, *A24*, 351−359.

Table 3. Atomic Positional Parameters and Equivalent Isotropic Thermal Parameters for $[Fe_5(\mu_3\text{-}F)_2(XDK)_2(N\text{-}MeIm)_4(O_2CPh)_4]\cdot 2Et_2O$ ($2\cdot 2Et_2O$)[a]

atom	*x*	*y*	*z*	B_{eq}[b]	atom	*x*	*y*	*z*	B_{eq}[b]
Fe(1)	0.92248(5)	0.21746(7)	0.02994(5)	2.24(4)	C(22a)	1.0296(9)	−0.304(1)	0.1161(9)	3.1(4)
Fe(2)	0.84286(5)	−0.00564(7)	0.04602(5)	2.40(4)	C(22b)	1.0287(8)	−0.284(1)	0.1384(8)	2.1(3)
Fe(3)	1.000	0	0	2.64(6)	C(23b)	1.0436(9)	−0.359(1)	0.1838(9)	4.1(4)
F(1)	0.9277(2)	0.0665(3)	0.0325(2)	2.6(2)	C(23a)	1.0339(7)	−0.396(1)	0.1422(7)	2.6(3)
O(10)	1.0197(2)	0.2316(4)	0.0620(3)	3.4(2)	C(24b)	1.0001(9)	−0.381(1)	0.2236(9)	4.6(4)
O(11)	1.0729(2)	0.0896(4)	0.0630(3)	3.3(2)	C(24a)	0.9831(8)	−0.443(1)	0.1645(8)	3.9(4)
O(20)	1.0032(2)	−0.1137(3)	0.0694(3)	3.0(2)	C(25b)	0.9366(8)	−0.334(1)	0.2139(8)	3.9(4)
O(21)	0.8966(2)	−0.1227(3)	0.0772(3)	3.4(2)	C(25a)	0.9250(8)	−0.395(1)	0.1664(8)	3.9(4)
O(101)	0.8430(2)	0.2028(3)	−0.0453(2)	2.7(2)	C(26a)	0.9181(8)	−0.297(1)	0.1438(8)	3.3(3)
O(102)	0.7954(2)	0.0599(4)	−0.0380(2)	2.9(2)	C(26b)	0.9238(7)	−0.256(1)	0.1693(7)	2.5(3)
O(103)	0.7145(3)	0.3819(4)	−0.0726(3)	4.3(3)	C(101)	0.8077(3)	0.1319(5)	−0.0687(4)	2.7(3)
O(104)	0.6267(3)	0.0859(4)	−0.0582(3)	5.1(3)	C(102)	0.6506(4)	0.1413(6)	−0.0901(5)	4.0(4)
O(201)	0.8855(3)	0.2133(4)	0.1119(3)	3.4(2)	C(103)	0.6995(4)	0.3043(6)	−0.0991(5)	3.6(4)
O(202)	0.8440(3)	0.0690(4)	0.1300(2)	3.2(2)	C(104)	0.8384(4)	0.0847(6)	−0.1687(4)	3.2(3)
O(203)	0.8047(3)	0.4008(4)	0.1506(4)	5.8(3)	C(105)	0.6992(4)	0.3805(6)	−0.2044(5)	4.9(5)
O(204)	0.7103(3)	0.1190(4)	0.1917(3)	4.3(3)	C(106)	0.5951(4)	0.0527(8)	−0.1895(5)	6.6(5)
N(1)	0.9096(3)	0.3691(4)	0.0257(3)	2.5(3)	C(107)	0.7816(4)	0.1322(5)	−0.1424(4)	2.7(3)
N(2)	0.8552(3)	0.5056(5)	0.0248(3)	4.5(3)	C(108)	0.7711(4)	0.2355(5)	−0.1703(4)	2.9(3)
N(3)	0.7529(3)	−0.0734(4)	0.0518(3)	3.0(3)	C(109)	0.7041(4)	0.2841(6)	−0.1682(4)	3.4(3)
N(4)	0.6457(4)	−0.0744(7)	0.0473(5)	6.5(5)	C(110)	0.6470(4)	0.2163(6)	−0.1982(5)	4.7(4)
N(101)	0.6756(3)	0.2299(5)	−0.0639(4)	3.8(3)	C(111)	0.6534(4)	0.1224(6)	−0.1598(5)	4.2(4)
N(201)	0.7599(3)	0.2575(5)	0.1696(4)	3.5(3)	C(112)	0.7187(4)	0.0716(5)	−0.1641(4)	3.5(4)
C(1a)	0.855(1)	0.416(1)	0.031(1)	2.9(4)	C(201)	0.8750(3)	0.1457(6)	0.1482(4)	2.7(3)
C(1b)	0.8531(9)	0.411(1)	0.0073(9)	2.2(4)	C(202)	0.7547(4)	0.1791(6)	0.2093(4)	3.4(4)
C(2b)	0.9109(8)	0.511(1)	0.0724(8)	3.8(3)	C(203)	0.8074(4)	0.3326(6)	0.1856(5)	4.7(5)
C(2a)	0.9200(8)	0.529(1)	−0.0001(8)	3.2(3)	C(204)	0.9741(4)	0.1037(6)	0.2293(4)	4.1(4)
C(3a)	0.9507(7)	0.441(1)	0.0056(7)	2.3(3)	C(205)	0.7719(5)	0.1184(7)	0.3226(4)	5.0(5)
C(3b)	0.9483(8)	0.429(1)	0.0725(8)	3.4(3)	C(206)	0.8834(5)	0.4226(7)	0.2727(6)	6.6(6)
C(4)	0.8015(5)	0.5722(7)	0.0217(5)	5.7(5)	C(207)	0.9059(4)	0.1573(5)	0.2205(4)	2.7(3)
C(5)	0.7024(4)	−0.0252(6)	0.0644(5)	4.7(4)	C(208)	0.8651(4)	0.1107(6)	0.2636(4)	3.6(4)
C(6)	0.6605(5)	−0.1606(8)	0.0223(6)	6.0(6)	C(209)	0.8053(4)	0.1692(6)	0.2734(4)	3.7(4)
C(7)	0.7265(5)	−0.1593(7)	0.0266(5)	5.2(5)	C(210)	0.8280(5)	0.2693(7)	0.2981(5)	4.8(5)
C(8)	0.5799(5)	−0.032(1)	0.0491(8)	12(1)	C(211)	0.8597(4)	0.3220(6)	0.2487(5)	4.2(4)
C(10)	1.0709(4)	0.1780(6)	0.0726(4)	2.8(3)	C(212)	0.9198(4)	0.2635(6)	0.2391(4)	3.8(4)
C(11)	1.1350(4)	0.2301(6)	0.1003(3)	3.0(3)	C(301)	0.7168(4)	0.2438(5)	0.0520(5)	3.3(4)
C(12)	1.1342(4)	0.3253(8)	0.1183(5)	5.5(5)	C(302)	0.6655(4)	0.2544(6)	−0.0004(5)	4.0(4)
C(13)	1.1927(6)	0.374(1)	0.1436(6)	9.0(8)	C(303)	0.6047(5)	0.2921(8)	0.0051(5)	5.5(5)
C(14)	1.2517(5)	0.330(1)	0.1482(5)	7.2(7)	C(304)	0.5965(5)	0.3166(9)	0.0646(6)	6.9(6)
C(15)	1.2537(4)	0.235(1)	0.1307(5)	5.8(6)	C(305)	0.6470(5)	0.3089(8)	0.1205(5)	5.7(5)
C(16)	1.1957(4)	0.1850(6)	0.1071(4)	3.7(4)	C(306)	0.7071(4)	0.2696(6)	0.1123(5)	4.0(4)
C(20)	0.9560(3)	−0.1506(5)	0.0877(3)	2.3(1)	C(307)	0.5484(5)	0.301(1)	−0.0549(6)	8.3(7)
C(21a)	0.9700(8)	−0.252(1)	0.1191(8)	1.6(3)	C(308)	0.6382(5)	0.3399(8)	0.1866(6)	6.7(6)
C(21b)	0.969(1)	−0.231(1)	0.134(1)	2.8(4)					

[a] Numbers in parentheses are errors in the last significant digit. See Figure 1 and Figure S2 for atom-labeling scheme. [b] $B_{eq} = (4/3)[a^2\beta_{11} + b^2\beta_{22} + c^2\beta_{33} + 2ab\cos(\gamma)\beta_{12} + 2ac\cos(\beta)\beta_{13} + 2bc\cos(\alpha)\beta_{23}]$.

$[Fe_5(\mu_3\text{-}F)_2(XDK)_2(py)_4(\mu\text{-}OBz)_4]\cdot 4CH_2Cl_2$ ($1\cdot 4CH_2Cl_2$). A deep yellow crystal measuring 0.2 × 0.3 × 0.5 mm was mounted in Paratone N on the end of a quartz fiber with silicone grease. Examination of the crystal by ω scans of several low-angle reflections revealed the sample to be of satisfactory quality ($\Delta\bar{\omega}_{1/2} = 0.29°$). Data were collected at 193 K with the $\omega-2\theta$ scan technique. The positions of all non-hydrogen atoms were refined anisotropically, except for the aromatic carbon atoms of the benzoate and XDK ligands, which were refined by using isotropic temperature factors. The largest peak in the final difference Fourier map was 0.9 $e^-/Å^3$, located in the vicinity of a CH_2Cl_2 molecule in the lattice.

$[Fe_5(\mu_3\text{-}F)_2(XDK)_2(N\text{-}MeIm)_4(O_2CPh)_4]$ (2). A deep yellow block-shaped crystal with dimensions 0.3 × 0.4 × 0.4 mm was mounted in Paratone N on the end of a quartz fiber with silicone grease. The crystal quality was found to be acceptable based on ω scans of several low-angle reflections ($\Delta\bar{\omega}_{1/2} = 0.26°$). Data were collected at 163 K with the $\omega-2\theta$ scan technique. The positions of all non-hydrogen atoms were refined anisotropically, except for those of the disordered lattice Et_2O molecule, which were refined with isotropic temperature factors. The phenyl rings of the benzoate and XDK ligands were treated as rigid groups and also refined isotropically. The Et_2O molecule was disordered over two positions with one shared carbon atom C(402). This carbon atom was refined with isotropic thermal parameters at full occupancy, while the remaining electron density was modeled by C(401a), C(401b), O(401a), O(401b), C(403a), C(403b), C(404a), and C(404b), each with isotropic thermal parameters at half occupancy. A phenyl ring of a benzoate group and one of the *N*-methylimidazole ligands were disordered over two positions, both refined at half occupancy. The largest peak in the final difference Fourier map was 0.58 $e^-/Å^3$, located in the vicinity of the disordered Et_2O molecule.

Mössbauer Spectroscopy. Mössbauer spectra of polycrystalline samples of **1** (70 mg) and **2** (70 mg) dispersed in BN powder and a frozen methanol solution of **1** (45 mg in 1 mL) were obtained by using a conventional, constant acceleration spectrometer. The γ-ray source was ^{57}Co in a Rh matrix maintained at 300 K. Isomer shifts were referenced to iron metal at 300 K. Spectral parameters were determined by least-squares fitting of the experimental data to theoretically calculated spectra by assuming Lorentzian line shapes.

Magnetic Susceptibility Measurements. Variable temperature solid state magnetic susceptibility measurements of **1** (26 mg) and **2** (25 mg) were made by using a Quantum Design MPMS SQUID susceptometer equipped with a 5.5 T magnet. Samples were loaded in a drybox in gel capsules and suspended in plastic straws. The susceptibilities of the capsule and the straw were measured at the same fields and temperatures for accurate corrections of their contribution to the total measured susceptibility. Diamagnetic corrections of -1188.28×10^{-6} and -1192.52×10^{-6} $cm^3\ mol^{-1}$ for **1** and **2**, respectively, were calculated from Pascal's constants[38,49] and were applied. A total

(49) O'Connor, C. J. *Prog. Inorg. Chem.* **1982**, *29*, 203−283.

of 40 data points were collected at 5000 G in the temperature range from 4 to 300 K. The dependence of the magnetization versus the applied field was measured to ensure that the fields selected for the variable temperature studies of **1** and **2** were within the linear presaturation regime of the magnetization versus *H/T* curves for the two compounds. Least-squares fits were carried out by using the program Model2.[50]

Results and Discussion

Synthesis. The two pentanuclear complexes $[Fe_5(\mu_3\text{-}F)_2(XDK)_2(py)_4(O_2CPh)_4]$ (**1**) and $[Fe_5(\mu_3\text{-}F)_2(XDK)_2(N\text{-}MeIm)_4(O_2CPh)_4]$ (**2**) were assembled by reacting $[Fe(H_2O)_6](BF_4)_2$], the deprotonated dicarboxylate ligand XDK, H_2XDK = *m*-xylylenediamine bis(Kemp's triacid)imide, a nitrogen donor ligand, *N*-methylimidazole (*N*-MeIm) or pyridine (py), and tetramethylammonium benzoate in a 5:2:4:5 ratio in a mixture of CH_2Cl_2/MeOH. The slight excess of benzoate increased the yield of the reaction. Separation of the precipitated $Me_4N(BF_4)$ and $Et_3NH(BF_4)$ salts by filtration and subsequent layering of a solution of **1** in CH_2Cl_2 or a solution of **2** in CH_2Cl_2/MeOH with Et_2O afforded the two deep yellow pentanuclear complexes. Colorless crystals sometimes found as impurities in samples of **2** were identified by infrared spectroscopy as BF_4^- salts and/or the mononuclear complex $[Fe(HXDK)_2(MeOH)_2]$[42] and were separated by recrystallization of **2** from benzene/Et_2O. The fluoride ions in the two pentanuclear complexes **1** and **2** are derived from BF_4^-, the counterions of the iron(II) salt that was used as the starting material. Release of fluoride ions from BF_4^- is known to occur in the presence of basic ligands which capture the BF_3 moiety, and is often used as a strategy to prepare transition metal fluoride complexes.[51,52]

When the analogous reaction was carried out with imidazole (ImH) as the nitrogen donor ligand, a similar pentanuclear complex was not obtained. Instead, the dinuclear tricarboxylato-bridged complex $[Fe_2(\mu\text{-}O_2CPh)(XDK)(ImH)_2(O_2CPh)(MeOH)]$ was isolated.[25] Similar dinuclear complexes were obtained when *p*-toluate was used as the carboxylate with either *N*-MeIm, py, or ImH as the nitrogen donor ligands.[53]

Structural Studies. X-ray diffraction studies showed that the two complexes **1** and **2** are isostructural, but they crystallize in different space groups owing to differences in the lattice solvent content. In both compounds (Figure 1, Tables 3 and 4), the five iron atoms are arranged in two equivalent, nearly equilateral triangles with one vertex, Fe(3) located on a crystallographic inversion center, in common. The geometry at the central iron atom is octahedral, whereas five ligands are coordinated to each of the outer iron atoms (Fe(1), Fe(2), Fe(1*), Fe(2*)) affording a trigonal bipyramidal environment. A triply-bridging fluoride ion links the three iron ions located at the corners of each triangle. This fluoride ion is situated 0.18 Å (in **1**) and 0.17 Å (in **2**) out of the plane that generated by the five iron atoms. One carboxylate group from the benzoate ligand bridges pairs of iron atoms along two edges of the triangle (Fe(1)/Fe(3), Fe(2)/Fe(3), Fe(1*)/Fe(3), and Fe(2*)/Fe(3)), whereas the two carboxylate groups of XDK bridge the third pair of iron atoms (Fe(1)/Fe(2) and Fe(1*)/Fe(2*)). The coordination sphere of each trigonal bipyramidal five-coordinate center is completed by a nitrogen donor ligand, pyridine and *N*-methylimidazole in **1** and **2**, respectively.

(50) Vef, A. *Model2. Fit and Evaluation Program*; Institut für Anorganische und Analytische Chemie, Johannes-Gutenberg-Universität: Mainz, Germany, 1989.
(51) Ten Hoedt, R. W. M.; Reedijk, J. *Inorg. Chim. Acta* **1981**, *51*, 23−27.
(52) Zang, Y.; Jang, H. G.; Chiu, Y.-M.; Hendrich, M. P.; Que, L., Jr. *Inorg. Chim. Acta* **1993**, *213*, 41−48.
(53) Herold, S.; Lippard, S. J. Unpublished results.

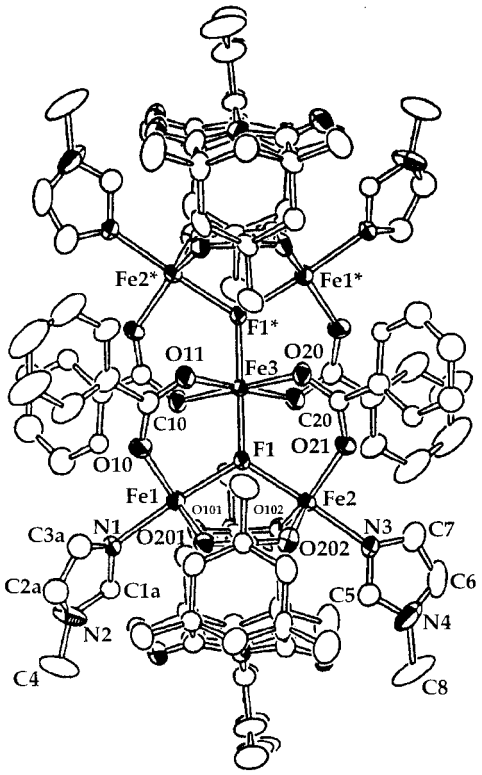

Figure 1. ORTEP plot of $[Fe_5(\mu_3\text{-}F)_2(XDK)_2(N\text{-}MeIm)_4(O_2CPh)_4]$ (**2**) showing the 50% probability thermal ellipsoids. For clarity, the hydrogen atoms are omitted.

Table 4. Selected Bond Lengths (Å) for $[Fe_5(\mu_3\text{-}F)_2(XDK)_2(py)_4(O_2CPh)_4]\cdot 4CH_2Cl_2$ (**1**·$4CH_2Cl_2$) and $[Fe_5(\mu_3\text{-}F)_2(XDK)_2(N\text{-}MeIm)_4(O_2CPh)_4]\cdot 2Et_2O$ (**2**·$2Et_2O$)[a]

atom	atom	**1**·$4CH_2Cl_2$	**2**·$2Et_2O$
Fe(1)	Fe(2)	3.569(4)	3.550(2)
Fe(1)	Fe(3)	3.452(3)	3.531(1)
Fe(2)	Fe(3)	3.484(3)	3.585(1)
Fe(1)	F(1)	2.075(6)	2.093(4)
Fe(1)	O(10)	2.005(8)	1.979(6)
Fe(1)	O(101)	2.018(7)	2.032(5)
Fe(1)	O(201)	2.051(8)	2.041(7)
Fe(1)	N(1)	2.15(1)	2.119(7)
Fe(2)	F(1)	2.086(6)	2.089(5)
Fe(2)	O(21)	2.014(7)	1.998(6)
Fe(2)	O(102)	2.030(8)	2.044(6)
Fe(2)	O(202)	2.043(8)	2.052(7)
Fe(2)	N(2)[b]	2.17(1)	2.114(7)
Fe(3)	F(1)	1.999(5)	1.999(5)
Fe(3)	O(11)	2.133(8)	2.168(6)
Fe(3)	O(20)	2.154(7)	2.141(6)

[a] Estimated standard deviations in the last significant figure are given in parentheses. See Figure 1 and Figure S1 for atom-labeling scheme. [b] N(3) for **2**.

The Fe···Fe distances are within a range of about 0.1 Å (Fe(1)···Fe(2) = 3.569(4) Å, Fe(1)···Fe(3) = 3.452(3) Å, and Fe(2)···Fe(3) = 3.484(3) Å in **1** and Fe(1)···Fe(2) = 3.550(2) Å, Fe(1)···Fe(3) = 3.531(1) Å, and Fe(2)···Fe(3) = 3.585(1) Å in **2**) and are only slightly longer than the Fe···Fe distance of 3.398(2) Å in the dinuclear complex $[Fe_2(\mu\text{-}F)(XDK)(N\text{-}MeIm)_2(MeOH)_3]$.[25] The average Fe−F−Fe angles are 119(2)° in **1** and 119(3)° in **2**. The average Fe−O bond lengths for the octahedral Fe(3) are significantly longer than those for the trigonal bipyramidal Fe(1) and Fe(2) ($Fe(1)-O_{av}$ = 2.02(2) Å, $Fe(2)-O_{av}$ = 2.02(2) Å, and $Fe(3)-O_{av}$ = 2.14(1) Å in **1** and $Fe(1)-O_{av}$ = 2.02(3) Å, $Fe(2)-O_{av}$ = 2.00(1) Å, and $Fe(3)-O_{av}$ = 2.14(1) Å in **2**), as expected on the basis of coordination number. On the other hand, the Fe(3)−F(1) bond

Table 5. Selected Bond Angles (deg) for $[Fe_5(\mu_3\text{-}F)_2(XDK)_2(py)_4(O_2CPh)_4]\cdot 4CH_2Cl_2$ (**1**·$4CH_2Cl_2$) and $[Fe_5(\mu_3\text{-}F)_2(XDK)_2(N\text{-}MeIm)_4(O_2CPh)_4]\cdot 2Et_2O$ (**2**·$2Et_2O$)[a]

atom	atom	atom	**1**·$4CH_2Cl_2$	**2**·$2Et_2O$
F(1)	Fe(1)	O(10)	94.4(3)	92.8(2)
F(1)	Fe(1)	O(101)	86.0(3)	87.1(2)
F(1)	Fe(1)	O(201)	89.8(3)	88.5(2)
F(1)	Fe(1)	N(1)	172.4(3)	175.7(2)
O(10)	Fe(1)	O(101)	146.2(3)	149.8(3)
O(10)	Fe(1)	O(201)	102.6(3)	104.3(3)
O(10)	Fe(1)	N(1)	88.2(4)	91.4(2)
O(101)	Fe(1)	O(201)	111.2(3)	105.8(2)
O(101)	Fe(1)	N(1)	87.9(3)	89.6(2)
O(201)	Fe(1)	N(1)	96.7(4)	89.6(3)
F(1)	Fe(2)	O(21)	93.0(3)	90.6(2)
F(1)	Fe(2)	O(102)	87.1(3)	85.7(2)
F(1)	Fe(2)	O(202)	87.1(3)	91.5(2)
F(1)	Fe(2)	N(2)[b]	175.5(3)	174.9(2)
O(21)	Fe(2)	O(102)	143.1(3)	141.0(3)
O(21)	Fe(2)	O(202)	111.3(3)	103.0(3)
O(21)	Fe(2)	N(2)[b]	90.8(4)	93.3(3)
O(102)	Fe(2)	O(202)	105.6(3)	115.9(2)
O(102)	Fe(2)	N(2)[b]	91.3(4)	89.2(3)
O(202)	Fe(2)	N(2)[b]	89.3(3)	90.9(3)
F(1)	Fe(3)	O(11)	88.7(3)	89.6(2)
F(1)	Fe(3)	O(20)	90.9(3)	90.9(2)
O(11)	Fe(3)	O(20)	94.1(3)	94.8(2)
Fe(1)	F(1)	Fe(2)	118.7(3)	116.2(2)
Fe(1)	F(1)	Fe(3)	117.5(3)	119.2(2)
Fe(2)	F(1)	Fe(3)	121.4(3)	122.5(2)

[a] Estimated standard deviations in the last significant figure are given in parentheses. See Figure 1 and Figure S1 for atom-labeling scheme. [b] N(3) for **2**.

(1.999(5) Å in both **1** and **2**) is significantly shorter than the Fe(1)−F(1) and Fe(2)−F(1) bonds (Fe(1)−F(1) = 2.075(6) and 2.093(4) Å, Fe(2)−F(1) = 2.086(6) and 2.089(5) Å in **1** and **2**, respectively). All these Fe−F bond lengths are considerably less than the corresponding bonds of the dinuclear complex $[Fe_2(\mu\text{-}F)(XDK)(N\text{-}MeIm)_2(MeOH)_3]$,[25] where the Fe−F distances are 2.238(5) and 2.169(5) Å for the six- and the five-coordinate iron centers, respectively.

A very similar structural motif occurs in the Cu(II) complex $[Cu_5(\mu_3\text{-}OH)_2(H_2O)(O_2CMe)_6(ImH)_4][ClO_4]_2$.[54] In this centrosymmetric compound, the three copper centers of each triangle are bridged by an acetate ligand and by a central, triply-bridging hydroxide ion. The coordination sphere of the two outer copper centers is completed by an imidazole and an imidazole and a bridging H_2O molecule, respectively. The pentanuclear units are linked symmetrically by these μ-aqua ligands forming a one-dimensional chain. A few other pentanuclear complexes with a similar arrangement of the metal ions but different types of bridging ligands have been reported. Included are the centrosymmetric nickel(II) complex $[Ni_5(\mu_3\text{-}OH)_2(L)_4(NO_2)_8(ImH)_4]$, where L = *N*-substituted ethane-1,2-diamines,[55] and the less symmetrical cobalt(II) complex $[Co_5(\mu_3\text{-}OH)_2(L)_4(acac)_8(NO_2)_2]$.[56,57] A last example is the pentanuclear iron(III) complex $[Fe_5(\mu_3\text{-}O)(L)_2(OH)_2(CH_3CO_2)_5(DMF)]$, where H_3L = 2,6-bis((salicylideneamino)methyl)-4-methylphenol, in which only one triply bridging oxo ligand is present.[58]

Although many high-nuclearity iron(III)[27−30] and mixed-valent iron(II)/iron(III)[31−34] complexes have been reported, the number of structurally characterized polynuclear iron(II) complexes is small. Examples of the largest aggregates include tetranuclear iron(II) complexes in which the four metal centers and four bridging oxygen donor ligands are arranged at alternating corners of a cube, as in $[Fe(OMe)(MeOH)(DBM)]_4$,[34] $[Fe(OMe)(MeOH)(DPM)]_4$,[34] and $[Fe_4(DBCat)_4(py)_6]$.[35] A different structural motif occurs in $[Fe_4(bpg)_3(O_2CPh)_3](ClO_4)_2$, a tetranuclear iron(II) complex in which the metal centers are bridged only by carboxylate ligands.[36] Two polynuclear *N*,*N*-dialkylcarbamate iron(II) compounds have been reported, the homoleptic $[Fe_6(O_2CNEt_2)_{12}]$ and the octanuclear complex $[\{Fe_4(\mu_4\text{-}O)(O_2CN^iPr_2)_6\}_2]$, resulting from the controlled hydrolysis of $[Fe_6(O_2CN^iPr_2)_{12}]$.[37]

Triply-bridging fluoride ions exist in a limited number of polynuclear metal complexes, mostly bound to alkali and alkaline earth metal ions.[59] An example of a transition metal complex in this class is the cubane-type cluster $[Co_4F_4(L)_{12}](BF_4)_4$ (L = *N*-ethylimidazole).[60] Although no examples of (μ_3-F)triiron(II) units were known at the inception of this work, we have since discovered that this motif is quite favored in polyiron(II) complexes. In particular, a trinuclear $\{Fe^{II}_3(\mu_3\text{-}F)\}$ complex and a tetranuclear iron(II) compound, in which two triply bridging fluoride ions and the four iron(II) ions are located at alternating corners of a cube, have recently been characterized.[53]

Mössbauer Spectroscopy. Zero-field Mössbauer spectra of polycrystalline samples of **1** and **2** were collected at 80 K. Figure 2 displays the traces and the theoretical least-square fits to the data. Both spectra show two overlapping doublets as revealed by a shoulder present in the spectrum of **1** and by the width and asymmetry of the obtained signals. The integrated absorption intensities of the two spectral subcomponents should reflect the relative population of iron in the two sites. The best fits to the data indicate the presence of inequivalent iron(II) centers in approximately a 4:1 ratio, in accord with the symmetry of the pentanuclear core revealed by crystallography. The isomer shifts for both doublets are similar, δ = 1.25−1.42 mm/s (Table 6). These values are within the range expected for high-spin iron(II) ions.[61] The quadrupole splitting parameters for both complexes are significantly different for the two sites, reflecting the different coordination environments of the two types of iron(II) ions. The central Fe(3) atom, which gives rise to the smaller ΔE_Q values (2.06 and 2.85 mm/s for **1** and **2**, respectively), has a more symmetrical octahedral coordination sphere compared to the more asymmetric pentacoordinate centers Fe(1), Fe(2), Fe(1*), and Fe(2*), which show larger ΔE_Q values (2.80 and 3.14 mm/s for **1** and **2**, respectively). Similar values have been obtained for other iron(II) complexes with inequivalent five- and six-coordinate sites.[18,62]

Solution Properties. Conductivity measurements of methanol solutions of **1** indicated partial dissociation of the anionic ligands to afford a species with properties between those of idealized 1:1 and 1:2 electrolytes (Figure S3). The zero-field Mössbauer spectrum of a frozen methanol solution of **1** was recorded at 4 K (Figure S4), and the data were fit to two inequivalent sites with parameters close to those obtained for the polycrystalline sample (Table 6). The major difference between the solution and the solid-state parameters is an increase

(54) Meenakumari, S.; Chakravarty, A. R. *J. Chem. Soc., Dalton Trans.* **1992**, 2305−2306.
(55) Finney, A. J.; Hitchman, M. A.; Raston, C. L.; Rowbottom, G. L.; White, A. H. *Aust. J. Chem.* **1981**, *34*, 2139−2157.
(56) Englert, U.; Strähle, J. *Z. Naturforsch.* **1987**, *B42*, 959−966.
(57) Abbreviations used are as follows: acac, acetylacetonate; DMF, dimethylformamide; HDBM, dibenzoylmethane; HDPM, dipivaloylmethane; $DBCatH_2$, 3,5-di-*tert*-butylcatechol; Hbpg, *N*,*N*-bis(2-pyridylmetyl)glycine.
(58) Mikuriya, M.; Nakadera, K. *Chem. Lett.* **1995**, 213−214.
(59) A search in the Cambridge Structural Database revealed only 11 examples of triply bridging fluoride complexes.
(60) Jansen, J. C.; van Koningsveld, H.; Reedijk, J. *Nature* **1977**, *269*, 318−319.
(61) Dickson, D. P. E.; Berry, F. J. *Mössbauer Spectroscopy*; Cambridge University Press: Cambridge, England, 1986.
(62) Rardin, R. L.; Bino, A.; Poganiuch, P.; Tolman, W. B.; Liu, S.; Lippard, S. J. *Angew. Chem., Int. Ed. Engl.* **1990**, *29*, 812−814.

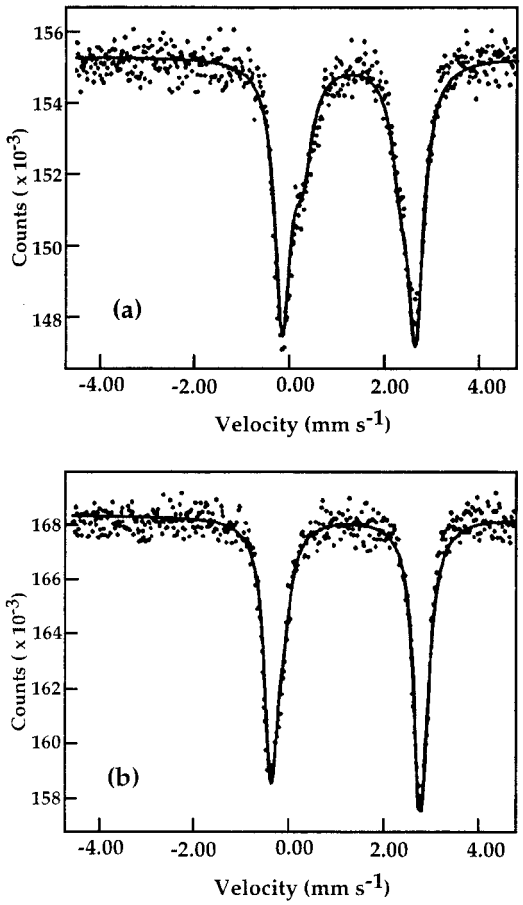

Figure 2. Mössbauer spectra at 80 K of polycrystalline (a) [Fe_5-(μ_3-F)$_2$(XDK)$_2$(py)$_4$(O_2CPh)$_4$] (**1**) and (b) [Fe_5(μ_3-F)$_2$(XDK)$_2$(*N*-MeIm)$_4$-(O_2CPh)$_4$] (**2**). The solid lines are the theoretical fits corresponding to the superposition of two inequivalent iron sites. See Table 6 for derived Mössbauer parameters.

Table 6. Mössbauer and Magnetic Parameters for [Fe_5(μ_3-F)$_2$(XDK)$_2$(py)$_4$(O_2CPh)$_4$] (**1**) and [Fe_5(μ_3-F)$_2$(XDK)$_2$(*N*-MeIm)$_4$(O_2CPh)$_4$] (**2**)

compd	δ, mm/s	ΔE_Q, mm/s	area, %	$-J_{12}$, cm^{-1}	$-J_{13}$, cm^{-1}
1	1.25	2.80	72	3.39(4)	3.26(4)
	1.30	2.06	28		
1 (in MeOH)[a]	1.26 (1.36)	2.93 (3.21)	76		
	1.22 (1.34)	2.27 (2.80)	24		
2	1.32	3.14	80	2.97(9)	2.56(8)
	1.42	2.85	20		

[a] Mössbauer data of a polycrystalline sample and a frozen MeOH solution collected at 4 K.

of the values of the quadrupole splitting for the two iron sites. In particular, ΔE_Q of the central iron ion is 2.27 mm/s for a polycrystalline sample and 2.80 mm/s for a MeOH solution of **1**. Such an increase indicates a less symmetrical coordination environment. These data, combined with the observation of some conductivity arising from the uncharged complex **1**, can be explained by assuming that the benzoate ligands are partially dissociated and replaced by solvent (MeOH) molecules. The fact that **1** can be recovered from these solutions in nearly quantitative yields further suggests that the integrity of the pentanuclear core is retained in MeOH.

Magnetic Properties. Variable temperature magnetic susceptibility data for the two pentanuclear compounds **1** and **2** were obtained at 5000 G. Plots of the effective magnetic moment per molecule as a function of temperature in the 4−300 K range are shown in Figure 3. The pyridine complex **1** has

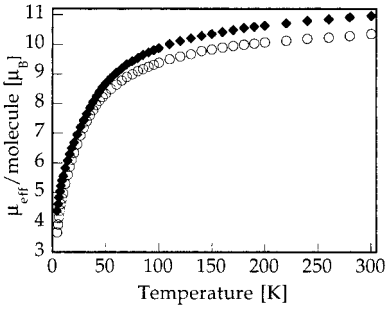

Figure 3. Plot of the effective moment (μ_{eff}) per molecule versus temperature for [Fe_5(μ_3-F)$_2$(XDK)$_2$(py)$_4$(O_2CPh)$_4$] (**1**) (◆) and [Fe_5-(μ_3-F)$_2$(XDK)$_2$(*N*-MeIm)$_4$(O_2CPh)$_4$] (**2**) (○).

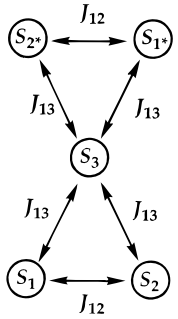

Figure 4. Diagram of the spin topology and magnetic exchange coupling pathway for the pentanuclear complexes.

an effective magnetic moment per molecule (μ_{eff}) which decreases from 10.98 μ_B at 300 K to 8.6 μ_B at 50 K whereupon there is a more rapid decrease to 4.4 μ_B at 4 K. The *N*-methylimidazole complex **2** has a μ_{eff} value of 10.38 μ_B at 300 K which decreases to 8.33 μ_B at 50 K and then more rapidly to 3.66 μ_B at 4 K. The μ_{eff} values at 300 K are close to the theoretical value of 10.95 μ_B calculated from the spin-only equation for the effective moment of five independent $S = 2$ iron(II) ions with $g = 2$. The decrease of μ_{eff} at lower temperatures indicates that the five high-spin iron(II) centers are antiferromagnetically coupled.

Considering the symmetry of **1** and **2**, two topologically distinct types of exchange pathways were proposed to evaluate their magnetic properties (Figure 4). The pathways are distinguished from one another by the nature of the bridging groups which link the iron centers. The first exchange interaction, J_{12}, involves the two centers Fe(1) and Fe(2), which are bridged by the two carboxylate groups of XDK and by the central triply bridging fluoride ion. The second coupling constant, J_{13}, defines the exchange interaction between Fe(1)/Fe(3) and Fe(2)/Fe(3), which are bridged by the same ligands, a benzoate group and the central fluoride ion. This exchange coupling scheme results in the spin-only isotropic Heisenberg Hamiltonian given in eq 1, where $S_i = 2$ and the numbering scheme for the S_iS_j terms is that used in Figure 4. An analytical expression for the

$$\boldsymbol{H} = -2\boldsymbol{J}_{12}(\boldsymbol{S}_1\cdot\boldsymbol{S}_2 + \boldsymbol{S}_{1*}\cdot\boldsymbol{S}_{2*}) - 2\boldsymbol{J}_{13}(\boldsymbol{S}_1\cdot\boldsymbol{S}_3 + \boldsymbol{S}_2\cdot\boldsymbol{S}_3 + \boldsymbol{S}_{1*}\cdot\boldsymbol{S}_3 + \boldsymbol{S}_{2*}\cdot\boldsymbol{S}_3) \quad (1)$$

eigenvalues of the Hamiltonian in eq 1 was derived by using the Kambé vector-coupling approach.[63] The intermediate coupling spin operators S_A, S_B, and S_C were defined as $\boldsymbol{S}_A = \boldsymbol{S}_1 + \boldsymbol{S}_2$, $\boldsymbol{S}_B = \boldsymbol{S}_{1*} + \boldsymbol{S}_{2*}$, and $\boldsymbol{S}_C = \boldsymbol{S}_A + \boldsymbol{S}_B$, and the total spin operator (S_T) becomes $S_T = S_C + S_3$. Equivalent operator

(63) Kambé, K. *J. Phys. Soc. Jpn.* **1950**, *5*, 48−51.

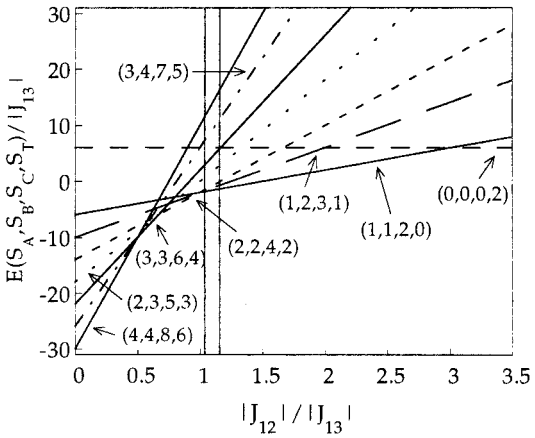

Figure 5. Plot of the relative energies $E/|J_{13}|$ versus $|J_{12}|/|J_{13}|$ for selected low-lying spin states. The numbers in parentheses correspond to the S_A, S_B, S_C, and S_T values for each state. The solid vertical lines delineate the values 1.04 and 1.16, calculated with the parameters obtained from the fits of the magnetic susceptibility data of **1** and **2**, respectively.

replacements can be made for all S_iS_j terms, and the original Hamiltonian can thus be rewritten as given in eq 2. The

$$\boldsymbol{H} = -2\boldsymbol{J}_{12}(\boldsymbol{S}_A^2 - \boldsymbol{S}_1^2 - \boldsymbol{S}_2^2 + \boldsymbol{S}_B^2 - \boldsymbol{S}_{1*}^2 - \boldsymbol{S}_{2*}^2) - 2\boldsymbol{J}_{13}(\boldsymbol{S}_T^2 - \boldsymbol{S}_C^2 - \boldsymbol{S}_3^2) \quad (2)$$

eigenvalues for this new Hamiltonian are given in eq 3, where the allowed values of S_A, S_B, S_C, and S_T are obtained by the addition rule of two spin vectors.[64] The total number of energy

$$E(\boldsymbol{S}_A,\boldsymbol{S}_B,\boldsymbol{S}_C,\boldsymbol{S}_T) = -\boldsymbol{J}_{12}[\boldsymbol{S}_A(\boldsymbol{S}_A+1) + \boldsymbol{S}_B(\boldsymbol{S}_B+1)] - \boldsymbol{J}_{13}[\boldsymbol{S}_T(\boldsymbol{S}_T+1) - \boldsymbol{S}_C(\boldsymbol{S}_C+1)] \quad (3)$$

levels for a system of five high-spin iron(II) ions ($S = 2$) is $(2S+1)^5 = 3125$. Because of the symmetry of the molecule, the overall degeneracy is distributed over 169 unique states with S_T values ranging from $S_T = 0$ to 10. By using eq 3, values of the relative energies of the possible spin states, $E/|J_{13}|$, can be calculated and plotted as a function of the ratio of the coupling constants $|J_{12}|/|J_{13}|$. Figure 5 displays such a plot for a few selected low-lying spin states. This correlation diagram shows that for $|J_{12}|/|J_{13}| > 3$, the ground state is $(S_A,S_B,S_C,S_T) = (0,0,0,2)$. For the cases where $3 > |J_{12}|/|J_{13}| > 1$, the lowest spin state of the pentanuclear cluster is (1,1,2,0). For $|J_{12}| > |J_{13}|$ several energy level crossings show that the ground state changes with small variations of the $|J_{12}|/|J_{13}|$ ratio. All these energy levels represent high-spin states with $S_T = 2$, 4, or 6, the value of the total spin increasing as $|J_{12}|/|J_{13}|$ approaches zero.

The energy levels (E_n) obtained with eq 3 were inserted into the van Vleck equation (eq 4),[38,65] where $\sum_n(m_{sn})^2 = {}^1/_3\boldsymbol{S}_T(\boldsymbol{S}_T+1)(2\boldsymbol{S}_T+1)$, to give the expression of the molar magnetic susceptibility (χ_M) versus temperature, which was used to fit the experimental data. The result of the best fit for **2** is shown in Figure 6. The final parameters for this fit were $J_{12} = -2.97(9)$ cm^{-1}, $J_{13} = -2.56(8)$ cm^{-1}, and $g = 2.04(2)$. No

$$\chi_M = \frac{Ng^2\mu_B^2}{kT}\frac{\sum_n(m_{sn})^2\exp(-E_n/kT)}{\sum_n(2S_T+1)2\exp(-E_n/kT)} \quad (4)$$

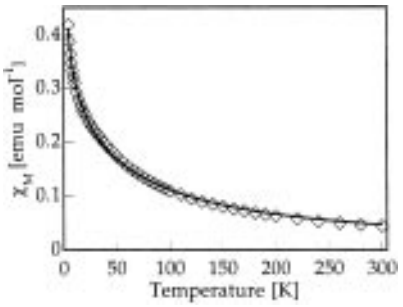

Figure 6. Plot of the molar susceptibility (χ_M) versus temperature for $[Fe_5(\mu_3\text{-}F)_2(XDK)_2(N\text{-}MeIm)_4(O_2CPh)_4]$ (**2**). The solid line corresponds to the best fit, obtained with the model described in the text.

corrections for paramagnetic impurities or temperature independent paramagnetism were applied. A good fit (Figure S5) and very similar parameters were obtained from the magnetic susceptibility data collected for **1**. During the fitting procedure, the g-value was kept fixed at $g = 2.2$ and the resulting values of the coupling constants were $J_{12} = -3.39(4)$ cm^{-1} and $J_{13} = -3.26(4)$ cm^{-1}. The $|J_{12}|/|J_{13}|$ ratio, which alone determines the ground state and the sequence of the excited states, is 1.04 and 1.16 for **1** and **2**, respectively. As shown in Figure 5, in which these two values are denoted by solid vertical lines, for both complexes the ground state energy level is the $S_T = 0$ state $(S_A,S_B,S_C,S_T) = (1,1,2,0)$. The orbital pathway for the two exchange interactions described by J_{12} and J_{13} probably involves the bridging fluoride ligand predominantly, which would explain the very similar values for the two coupling constants obtained for both **1** and **2**. No satisfactory fits of the experimental susceptibility data could be achieved by setting $J_{12} = J_{13}$, however, an even more simplified model employing only one type of exchange pathway to describe the magnetic interactions in the molecule.

An attempt to estimate the total ground spin state (S_T) for both **1** and **2** was made by extrapolating μ_{eff} to 0 K from the lowest temperature portion of the μ_{eff} versus temperature curves (Figure S6). For **1**, the extrapolated value of μ_{eff} to 0 K is 3.45 μ_B. This value lies between those of 4.9 and 2.8 μ_B, calculated from the spin-only equations for the effective moment for $g = 2$ and a total spin $S_T = 2$ and $S_T = 1$, respectively. Extrapolation of the low-temperature μ_{eff} plot for **2** gave a value of 2.84 μ_B at 0 K, which corresponds closely to that of 2.8 μ_B calculated for a spin of $S_T = 1$ and $g = 2$. Both complexes have complicated low-lying magnetic structures with a ground state that is not well isolated and lies only a few wavenumbers below the first excited states and having higher total spins, $S_T = 1$, 2, or 3 (Figure 7). This result reflects spin frustration in the molecules since, even though all pairwise magnetic exchange interactions are antiferromagnetic, the topology of the complex does not allow the lowest spin state to be the ground state.[66−68] The higher ground states that are observed may be due to spin frustration or to contributions from the zero-field splitting, which are probably significant owing to the small values of the coupling constants. A field-dependent magnetization study at low temperature would further reveal the nature of the ground state.

(64) Kahn, O. *Molecular Magnetism*; VCH Press: New York, 1993.
(65) van Vleck, J. H. *The Theory of Electric and Magnetic Susceptibilities*; Oxford University Press: London, 1932.
(66) McCusker, J. K.; Christmas, C. A.; Hagen, P. M.; Chadha, R. K.; Harvey, D. F.; Hendrickson, D. N. *J. Am. Chem. Soc.* **1991**, *113*, 6114−6124.
(67) McCusker, J. K.; Vincent, J. B.; Schmitt, E. A.; Mino, M. L.; Shin, K.; Coggin, D. K.; Hagen, P. M.; Huffman, J. C.; Christou, G.; Hendrickson, D. N. *J. Am. Chem. Soc.* **1991**, *113*, 3012−3021.
(68) Christmas, C. A.; Tsai, H.-L.; Pardi, L.; Kesselman, J. M.; Gantzel, P. K.; Chadha, R. K.; Gatteschi, D.; Harvey, D. F.; Hendrickson, D. N. *J. Am. Chem. Soc.* **1993**, *115*, 12483−12490.

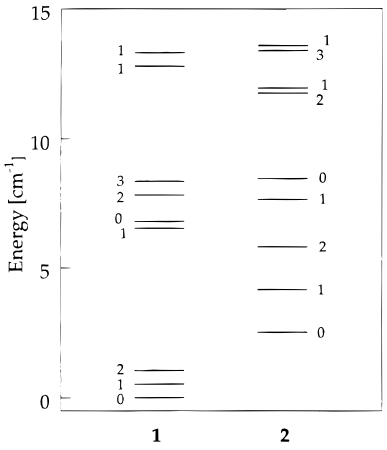

Figure 7. Plot of the distribution of the energy of the lowest spin states for 1 and 2. The ground state energy of **1** has arbitrarily been set equal to zero, and the value of the corresponding total spin (S_T) is displayed beside each level.

The simplified model of exchange coupling applied in this study assumes Heisenberg exchange between all spins and thus does not take into account the single-ion anisotropy of the iron(II) centers. Furthermore, the analysis does not incorporate spin−orbit coupling and zero-field interactions, which often are not negligible in the case of iron(II) ions. A more detailed analysis, including a term for the zero-field splitting, would require a considerably more complex theoretical treatment beyond the scope of the present investigation. Thus, although to a first approximation satisfactory fits of the experimental data to the simplified model were obtained, we do not completely exclude the possibility that no Heisenberg exchange is present in the complexes and that the magnetism is induced by the applied magnetic field.

Summary and Conclusions

The two compounds described in this paper are the first examples of pentanuclear iron(II) complexes. The X-ray analyses revealed highly symmetrical structures in which five iron atoms are situated on the corner of two triangles sharing a vertex. The central iron atom is located on a crystallographic inversion center. A triply bridging fluoride ion in the center of each triangle is another novel feature of these two structures. In the Mössbauer spectra, the five-coordinate peripheral and the central, octahedrally coordinated, iron atoms give rise to two overlapped doublets, with similar isomer shifts but slightly different quadrupole splitting parameters, reflecting the distinct symmetry of the two types of iron centers. A slight increase of the values of the quadrupole splitting observed for a frozen solution of **1** is attributed to partial displacement of the benzoate ligands by the solvent (MeOH), which leads to a less symmetrical coordination environment of the central iron ion. Such dissociation is supported by conductivity measurements that indicate the presence, in solution, of a species with properties between a 1:1 and a 1:2 electrolyte.

According to the symmetry of the molecule, two exchange pathways were introduced to explain the magnetic interactions between the five iron atoms. By using the Kambé vector-coupling approach, it was possible to obtain an analytical expression for the energy levels, resulting from the Hamiltonian corresponding to this exchange coupling scheme. The results of the fits of the magnetic susceptibility data indicated that two weak antiferromagnetic coupling constants determine the magnetic interactions in the two complexes. The theoretical ground state, calculated by applying the J values obtained from the simplified fits, has a total spin of zero and was not experimentally achieved. This result may be due to zero-field splitting effects, to spin frustration, or to deficiencies in the theoretical model.

Acknowledgment. This work was supported by grants from the National Institute of General Medical Sciences and AKZO. S.H. thanks the Swiss National Science Foundation and the Jubiläums-Stiftung (Ciba-Geigy, Basel) for postdoctoral fellowships. We are grateful to Dr. G. P. Papaefthymiou for collecting and fitting the Mössbauer data and Dr. D. P. Goldberg for useful discussion.

Supporting Information Available: Tables S1−S8, listing atomic coordinates and B_{eq}, anisotropic thermal parameters, and intramolecular bond distances and angles for **1** and **2** and Figures S1−S6 representing an ORTEP plot of **1**, the numbering scheme for the XDK ligand, conductivity data for MeOH solutions of **1**, the Mössbauer spectrum at 4 K of a frozen MeOH solution of **1**, a plot of the molar susceptibility (χ_M) versus temperature, together with the best fit, for **1** and the extrapolation curves to 0 K of the μ_{eff} plots of **1** and **2** (32 pages). Ordering information is given on any current masthead page.

IC960783I